이학석사 학위논문

Interannual to decadal variability of the Kuroshio shelf intrusion and associated changes in the East China Sea

동중국해 쿠로시오 대륙붕 유입의 장주기 변동성

2020년 2월

서울대학교 대학원

지구환경과학부

강 지 원

Abstract

Interannual to decadal variability of the Kuroshio shelf intrusion and associated changes in the East China Sea

Jiwon Kang

School of Earth and Environmental Sciences

The Graduate School

Seoul National University

A westward shift of the Kuroshio toward the continental shelf in the East China Sea (ECS) contributes an exchange of different water masses between the western boundary current and the shelf region, and plays a key role in the regional ecosystem and climate over the ECS. The Kuroshio shelf intrusion (KSI) is known to occur during winter associated with the weakening of the Kuroshio east of Taiwan. This study reveals that interannual to decadal variability of the KSI is as significant as the seasonal variability, and investigates the long-term KSI associated changes in the ECS by analyzing various datasets including 25-year-long satellite altimetry, high-resolution ocean reanalysis products, surface drifters, etc. A series of composite analysis confirms that the KSI is related to the strengthening of

the northeasterly wind, increase of the upward heat flux and overall surface warming in the ECS. Subsurface temperature, however, decreases in the shallow shelf region during the KSI events, possibly due to the topographic effect. Sub-mesoscale eddy kinetic energy (EKE) exhibits increase in the shelf region during the KSI, whereas the mesoscale EKE does not show significant changes associated with the KSI.

Keywords: Kuroshio shelf intrusion (KSI), East China Sea (ECS), Subsurface temperature, Sub-mesoscale eddy, Eddy kinetic energy (EKE)

Student Number: 2018-25621

Table of Contents

List of Figures

1. Introduction

The Kuroshio, one of the western boundary currents in the North Pacific (Nitani, 1972), flows northeastward along the Okinawa trough in the southern East China Sea (ECS) (Figure 1). A westward (or onshore) shift of the Kuroshio toward the continental shelf is referred to as the Kuroshio shelf intrusion (KSI) or onshore intrusion (Guo et al., 2006; Tang & Yang, 1993). The KSI induces an exchange of water masses and nutrients between the deep western boundary current region and the shallow continental shelf region, and thus changes hydrographic properties in the ECS (Chen et al., 1995; Tang et al., 1999). The KSI is responsible for the changes in the regional ocean circulation (Vélez-Belchí et al., 2013; Yang et al., 2018a), climate (Wu et al., 2014), and even fisheries (Sassa et al., 2006) over the ECS.

The path of the Kuroshio is relatively straight along the Okinawa trough when the Kuroshio is strengthened east of Taiwan, whereas it meanders toward the shelf region when the upstream Kuroshio is weak (Liu & Gan, 2012; Wu, 2013). Previous studies found out that the KSI occurs more frequently and tends to become stronger in winter when the Kuroshio is weak (Figure 2a), compared to summer (Figure 2b) (Chuang & Liang, 1994; Guo et al., 2003). The intensity of the Kuroshio east of Taiwan is known to be seasonally modulated by the relative number of cyclonic and anti-cyclonic eddies propagating from the North Pacific (Yin et al., 2019).

The westward propagation of the eddies is also related to the intra-seasonal variability of the Kuroshio; arrival of cyclonic eddies east of Taiwan weakens the Kuroshio with about 100-day interval (Johns et al., 2001; Lee et al., 2013; Vélez-Belchí et al., 2013; Yang et al., 1999; Zhang et al., 2001). Moreover, Wu et al., (2017) proposed that the frequent occurrence of the KSI during 2002–2013 compared to 1993–2001 is due to the decadal changes in the eddy kinetic energy (EKE), which is based on the mesoscale (~ 1/4º) data analysis.

Recent in-situ observations (Chern et al., 1990), analysis of long-term satellite altimetry (Hsin et al., 2013; Wang & Oey, 2014; Wu et al., 2014), and model simulations (Liu et al., 2014) have reported that the weakening of the Kuroshio and the strengthening of the KSI in the ECS is associated with the strengthening of northeasterly wind stress, surface heat loss, and shelf warming over the ECS. A snapshot in-situ observation by Yang et al. (2018a) showed that while the KSI induces increase of sea surface temperature (SST) over the shelf of the ECS, the subsurface temperature decreases in the onshore region during the KSI event. The surface warming and subsurface cooling would be an important factor for the exchange of heat and momentum between the deep western boundary current and shallow shelf region, and require to be investigated on the long-term basis. The changes in the EKE associated with the KSI also needs to be further studied particularly including the sub-mesoscale variability, as Liu et al.

(2017) pointed out that there are more sub-mesoscale eddies than mesoscale eddies in the ECS.

The present study investigates the interannual to decadal variability of the KSI in the ECS based on the long-term data analysis during 1993–2017. Two main questions to explore include 1) whether the subsurface cooling during the KSI event reported by the snapshot observation is found from the 25-year data analysis or not, 2) how does sub-mesoscale EKE change in comparison with the mesoscale EKE during the KSI events. Section 2 describes the data used in this study and the KSIS index derived from the 25-year-long satellite altimetry. The interannual to decadal variability of the KSI and its associated changes in the East China Sea is investigated in Section 3. Discussion and conclusions follow in Section 4.

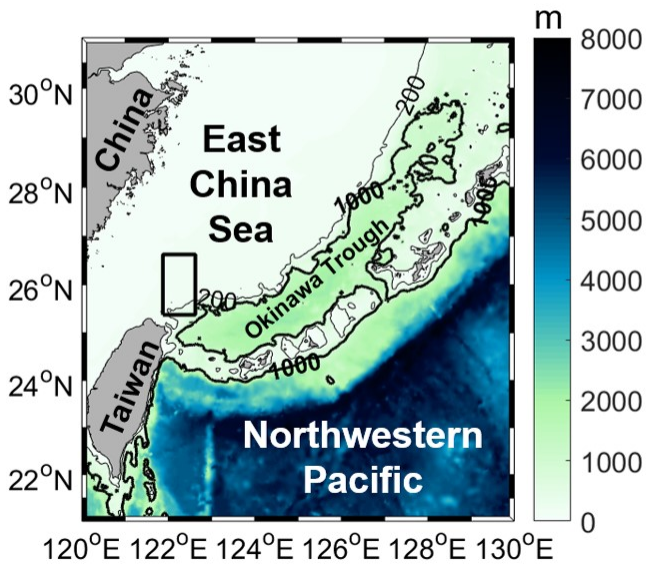

Figure 1. Bathymetry of the East China Sea and the Northwestern Pacific. 200 and 1000 m depths are shown in black contours.

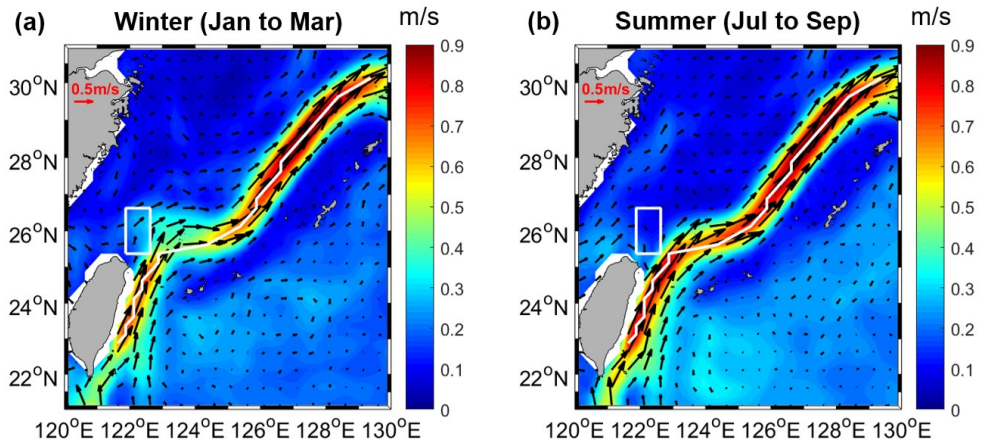

Figure 2. 25-year mean geostrophic current velocities in vectors and speed in shading. **(a)** Winter (January to March) **(b)** Summer (July to September).

2. Data and Methods

2.1. Data

Daily geostrophic velocities based on the satellite altimetry were obtained from Copernicus Marine Environment Monitoring Service (http://marine.copernicus.eu). EKE is calculated from 40–200 days band-pass filtered daily geostrophic velocities which is related to the time scales of eddy activity, and then monthly averaged.

Daily upper 10-meter winds were from Cross-Calibrated Multi-Platform version 2.0, which is reconstructed by using outputs from satellites, moored buoys, and modeling (http://www.remss.com/measurements/ccmp). Daily SST data were provided from Optimal Interpolation Sea Surface Temperature, which is produced by combining several observation platforms including satellites, ships, and buoys (https://www.ncdc.noaa.gov/oisst/data-access). Geostrophic velocities, winds, and SST were converted from daily to monthly mean with a spatial resolution of 0.25°. Wind stress and wind stress curl were calculated from the monthly-averaged 10-meter winds (Large & Fond, 1980; Trenberth et al., 1990). In addition, surface heat flux was obtained from monthly Objectively Analyzed air-sea flux (OAflux) with a spatial resolution of 1° (http://oaflux.whoi.edu), and turbulent heat flux is calculated as the sum of sensible and latent heat flux. All the above data were set to the same time period from 1993 to 2017 (25 years).

Three-dimensional ocean temperature, salinity, and currents are provided by Four-dimensional variational ocean reanalysis for the western North Pacific over 30 years (FORA-WNP30) from 1993 to 2014 (http://www.godac.jamstec.go.jp/catalog/data_catalog/metadataDisp/FORA-WNP30?lang=en). This high-resolution (0.1°) reanalysis products can resolve sub-mesoscale variability (Usui et al., 2017), and the surface current were used to investigate the sub-mesoscale variability in the ECS. Surface current and upper 200 m temperature and salinity (17 vertical levels) were converted from daily to monthly means during the 22 years over the ECS. Surface drifter data were provided from Global Drifter Program (GDP) database (https://www.aoml.noaa.gov/phod/gdp) during 1993–2017, which was quality-controlled and interpolated every 6 hours (Lumpkin and Centurioni, 2019). The GDP surface drifters provide additional information on the sub-mesoscale eddies that is not resolved by satellite altimetry due to the spatial resolution (Dong et al., 2011; Liu et al., 2017).

2.2. KSIS index

Monthly geostrophic speed was calculated from the geostrophic velocities, and the geostrophic speed anomalies were obtained after removing their monthly climatology and 13 months low-pass filtered during 1993–2017. Empirical Orthogonal Function (EOF) analysis (North, 1984) was then conducted for the geostrophic speed anomalies over the KSI

domain (121.875°E–122.625°E, 25.375°N–26.625°N, Figure 3a). Figure 3 shows the first EOF mode that explains about 62.4% of the interannual to decadal variability. The spatial pattern displays an increase of the geostrophic speed over the KSI domain, which represents the KSI. The principal component (PC) time series of the first mode was thus used as the KSIS index. The positive (negative) phase of the KSIS index indicates the time period of the KSI (non-KSI) (Figure 3c). The composite analysis was conducted for the ocean environmental variables by using the KSIS index, in order to understand the KSI-related changes over the ECS based on the comparison between the KSI and the non-KSI. Wind, surface heat flux, temperature, and EKE are applied to the composite analysis.

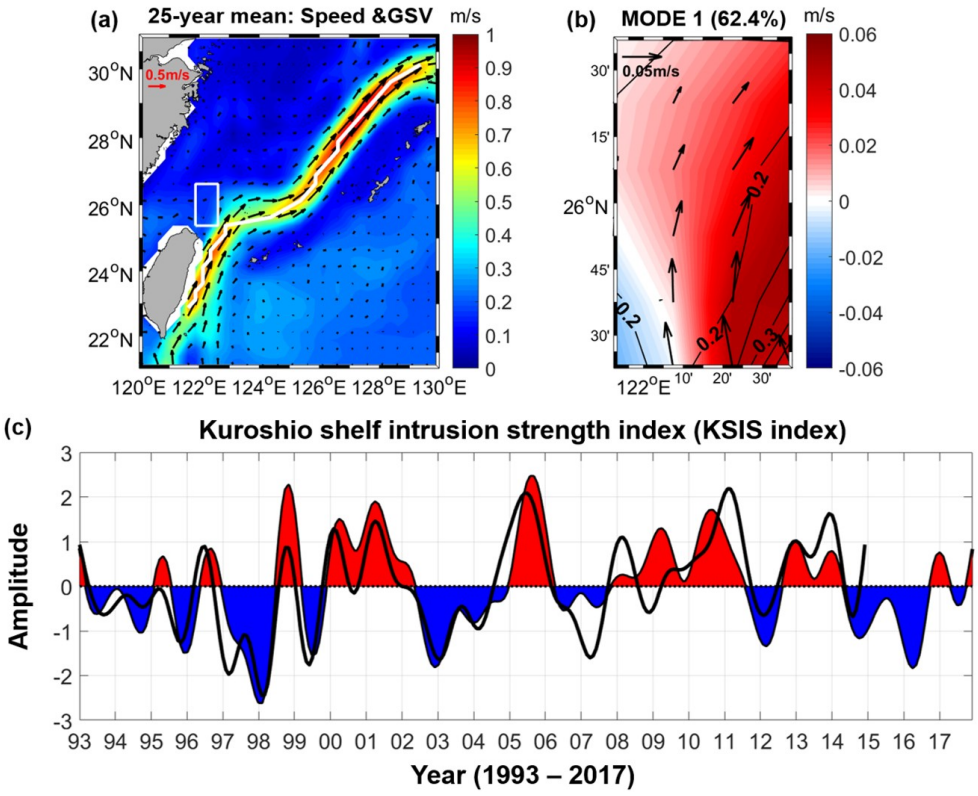

Figure 3. (a) 25-year mean geostrophic current velocities in vectors and speed in shading. White box denotes the KSI domain used for applying the EOF analysis, and white line displays the Kuroshio main axis computed from the location of maximum current speed (Guo et al., 2012; Kamachi et al., 2004). **(b)** Spatial pattern of the first EOF mode of geostrophic current anomalies in the KSI domain. **(c)** The corresponding PC time series of the first EOF mode, the KSIS index. The black thick line denotes PC time series of the first EOF mode of geostrophic current anomalies based on FORA-WNP30.

3. Results

3.1. Interannual to decadal variability of the KSI

Figure 4a shows positive composites of the geostrophic current speed and velocities based on the KSIS index. The main axis of the Kuroshio is computed from the location of maximum current speed for the period of 1993–2017 (Guo et al., 2012; Kamachi et al., 2004). In the KSI domain, positive speed anomalies and north(east)ward vector anomalies are observed, while negative speed anomalies and south(west)ward vector anomalies are seen east of Taiwan and to the east of the Kuroshio main axis (Figure 4a). Negative composites display opposite signs of the anomalies and direction of the current vector (Figure 4c). The sum of the anomalies and the 25-year mean show the difference of the current between the KSI and non-KSI; the north(east)ward current and its speed increase in the KSI domain, and the Kuroshio weakens during the KSI (Figures 4b and 4d). The path of the Kuroshio gives a hint of meandering during the KSI, while it is relatively straight along the Okinawa trough during the non-KSI. This result is consistent with the previous studies that showed the KSI (non-KSI) occurs with the weakening (strengthening) of the Kuroshio east of Taiwan (Guo et al., 2006; Wu et al., 2014).

Figures 5a and 5b show positive and negative composites of wind stress and wind stress curl anomalies based on the KSIS index. In comparison with the 25-year mean (Figure 5c), the composites indicate that

northeasterly wind stress is strengthened (weakened) over the ECS during the KSI (non-KSI). The northeasterly wind anomalies induce westward Ekman transport (Figure 5a), which would be associated with the westward shift of the Kuroshio in the ECS (Guo et al., 2006). The westward shift, thus the weakening of the Kuroshio is then linked to the KSI. On the contrary, the weakened northeasterly wind stress tends to suppress the westward shift of the Kuroshio during the non-KSI (Figure 5b). Wang & Oey (2014) also suggested that the strengthened northeasterly wind is the most important contributor to the KSI.

Changes in the surface turbulent heat flux during the KSI are investigated, considering that the KSI is related to the interaction between the ocean and atmosphere (Sasaki et al., 2017; Wu et al., 2014). In the composites of surface heat flux, positive values denote the anomalous heat flux from ocean to atmosphere (Figures 5d-5f). The upward turbulent heat flux is strengthened (weakened) over the ECS during the KSI (non-KSI). Likewise, the positive and negative composites of SST anomalies are displayed in Figures 5g and 5h. The SST also increases over the ECS during the KSI. The increase of the upward heat flux and SST are consistent with the results by Wang & Oey (2014). Composites of the mesoscale EKE anomalies based on the satellite altimetry data show the KSI-associated changes in Figures 5j and 5k, in comparison with the 25-year mean in Figure 5i. They do not exhibit significant variations in the ECS including the KSI domain between the KSI and non-KSI.

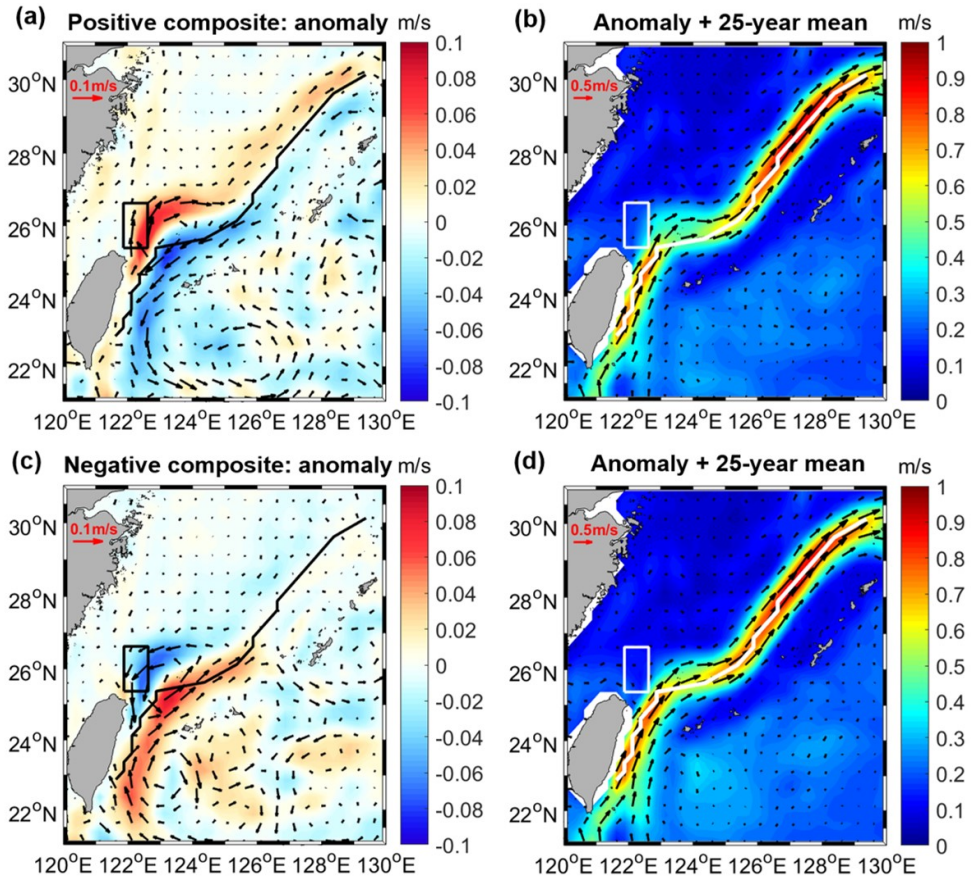

Figure 4. (a,c) Positive and negative composites of the geostrophic current anomalies in vectors and speed anomalies in shading based on the KSIS index. **(b,c)** Sum of the anomalies and the 25-year mean. The black/white boxes and black/white lines denote the KSI domain and the Kuroshio main axis, same as in Figure 3a.

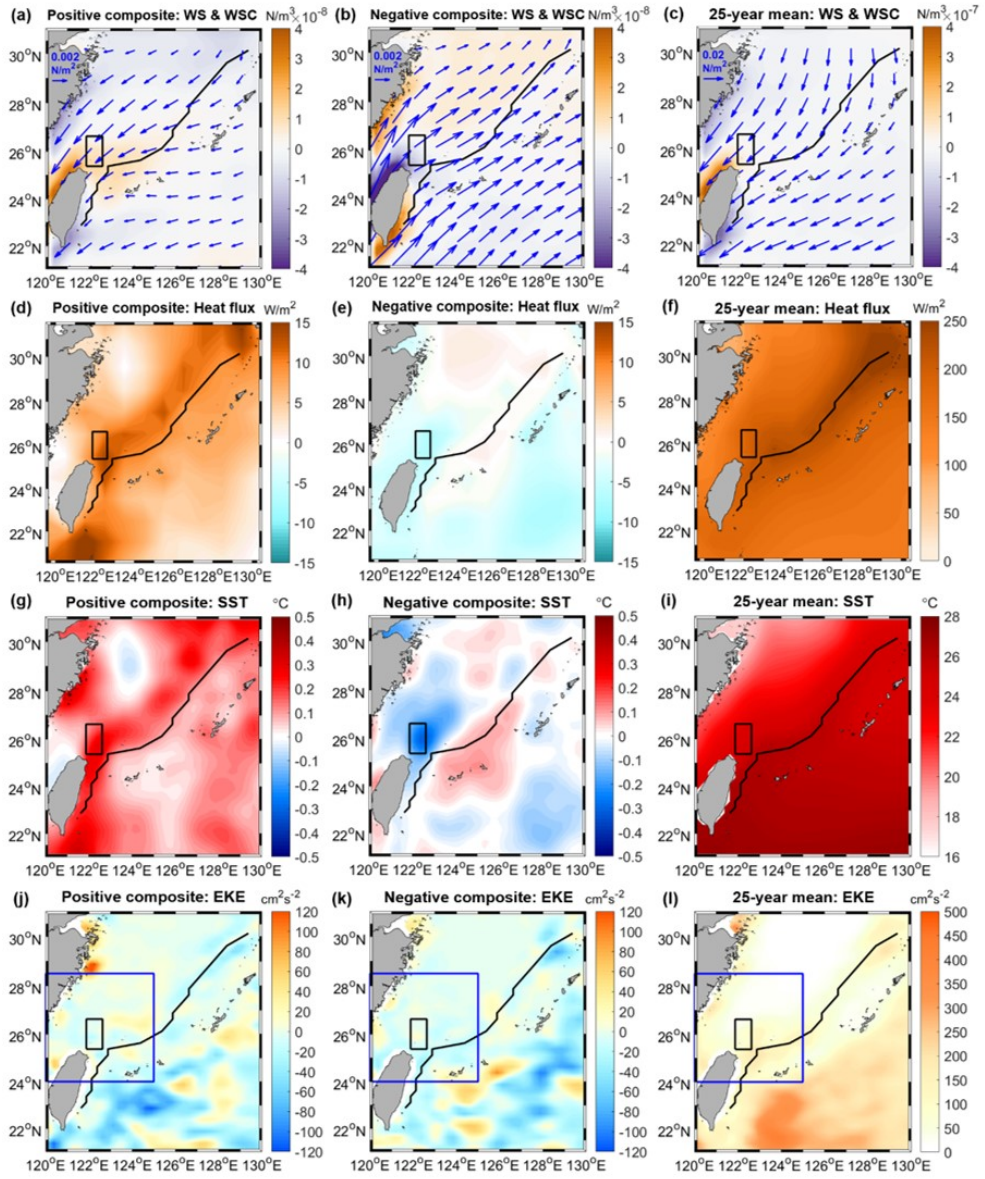

Figure 5. Positive and negative composites of anomalies based on the KSIS index, and 25-year mean of **(a-c)** wind stress (WS) in vectors and wind stress curl (WSC) in shading, **(d-f)** turbulent heat flux (sum of sensible and latent heat flux). Positive (negative) values of the turbulent heat flux denote upward (downward) surface heat flux. **(g-i)** Same but for sea surface temperature (SST). **(j-l)** Same but for mesoscale eddy kinetic energy (EKE) derived from satellite altimetry. Blue boxes indicate the shelf region seen in Figure 13.

3.2. Subsurface temperature variability

Figure 6 shows the changes in the near-surface and subsurface temperature at 0.5, 50, 100, and 200 m associated with the KSI. The near-surface temperature anomalies in Figures 6a and 6b display consistent patterns with the SST anomalies shown in Figures 5g and 5h. The temperature increases during the KSI is also observed in the subsurface layer over the Okinawa trough along the west of the Kuroshio main axis. However, subsurface cooling is seen in the continental shelf region north of the Taiwan at 50 and 100 m during the KSI (Figures 6d and 6g). The temperature anomalies exhibit opposite signs during the non-KSI compared to those during the KSI (Figures 6e and 6h). Temperature anomalies at 200 m is consistent with those at shallower depths, but limited to the Okinawa trough because the shelf region including the KSI domain is shallower than 200 m (Figures 6j-6l).

Vertical section of the temperature and temperature anomalies along line-A including the KSI domain is shown in Figure 7. The surface warming during the KSI is extended to the subsurface down to about 20-meter depth (Figure 7a), which is expected from the subsurface temperature anomalies presented in Figures 5g and 6a. Temperature anomalies deeper than 20-meter depth exhibit warming in the Okinawa trough during the KSI, but cooling in the continental shelf (Figure 7a). The negative subsurface temperature anomalies in the shelf region could be induced by the

topographic effect as the deep Okinawa trough is occupied by relatively cold water masses in the subsurface layer (Figure 7c) and the Kuroshio shifts shoreward from the deep western boundary current region to the shallow shelf region. Negative composites display opposite signs of the temperature anomalies in the subsurface layer of the shelf region (Figure 7b).

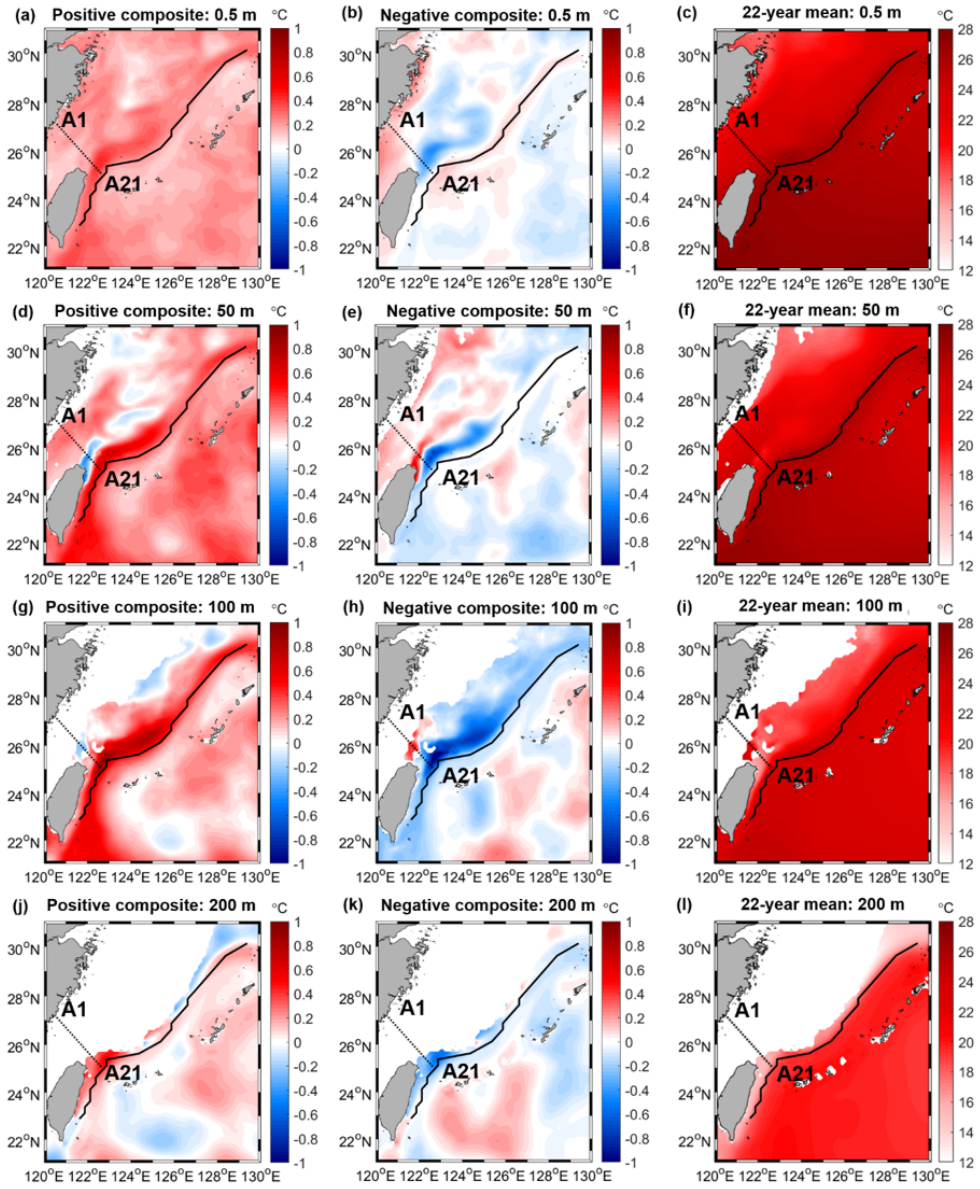

Figure 6. Positive and negative composites of temperature anomalies based on the KSIS index, and 22-year mean (1993–2014) of the temperature from FORA-WNP30 reanalysis. Line-A is aligned from A1 to A21. **(a-c)** 0.5 m. **(d-f)** 50 m. **(g-i)** 100 m. **(j-l)** 200 m. The black lines denote the Kuroshio main axis.

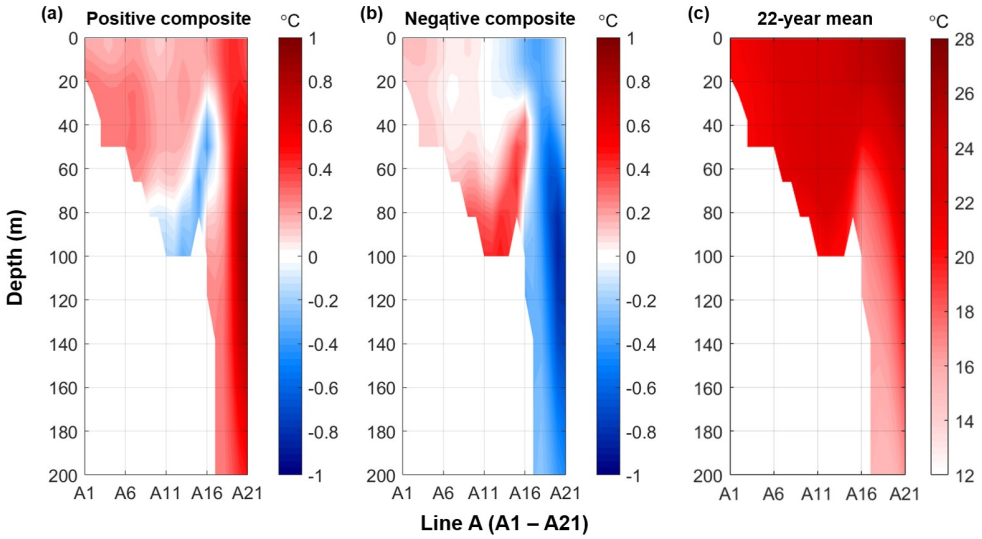

Figure 7. Vertical sections of (a) positive and (b) negative composites of temperature anomalies based on the KSIS index, and (c) 22-year mean of the temperature from FORA-WNP30 reanalysis. The line-A is shown in Figure 6.

3.3. Sub-mesoscale variability

Sub-mesoscale eddies, which have about an order smaller radius compared to mesoscale eddies, are known to be more abundant in the ECS (Liu et al., 2017). Because of the limited spatial resolution of the satellite altimetry, distribution of eddies including both mesoscale and sub-mesoscale variability related to the KSI is investigated by using the surface drifters. A total of 271 surface drifters are selected passing through the specific domain (122.125°E–124.875°E, 24.875°N–27.125°N) northeast of Taiwan, and their trajectories are displayed in Figure 8a. Sub-mesoscale eddies as well as mesoscale eddies are detected by using the lagrangian eddy detection scheme introduced by Dong et al. (2011).

Figure 8b shows the drifter trajectories of the detected cyclonic and anti-cyclonic eddies in different colors. As suggested in Liu et al. (2017), eddies may not be able to develop easily due to the interruption of the Ryukyu island which is located in the eastern part of the Kuroshio main axis. Therefore, more eddies exist on the western side of the Kuroshio than its eastern side in the ECS. Furthermore, most of the cyclonic eddies are distributed on the western side of the Kuroshio, whereas anti-cyclonic eddies are on the eastern side. This antisymmetric distribution of the cyclonic and anti-cyclonic eddies are consistent with the previous studies by Liu et al. (2017) and Qin et al. (2015). Figure 8c presents a histogram of the number of eddies in terms of eddy size (radius) and spinning direction. The

eddy size is up to 50 km radius in the ECS. There were 37 cyclonic eddies and 10 anti-cyclonic eddies in the ECS during 1993–2017, and most of them are sub-mesoscale eddies (up to 20 km radius).

The sub-mesoscale EKE variability associated with the KSI was examined by using FORA-WNP30 which is a sub-mesoscale-resolving reanalysis product. Figures 9a and 9b display the composites of EKE anomalies including sub-mesoscale variability according to the KSI. The EKE increases in the KSI domain and decreases to the western side of the Kuroshio during the KSI. On the other hand, it decreases in both regions during the non-KSI. The signs of EKE anomalies are slightly different from those of mesoscale EKE anomalies based on the satellite altimetry in Figures 5j-5l. As shown in Figures 9a and 9b, the amplitude of EKE anomalies including the sub-mesoscale variability is larger than those with mesoscale variability in the ECS.

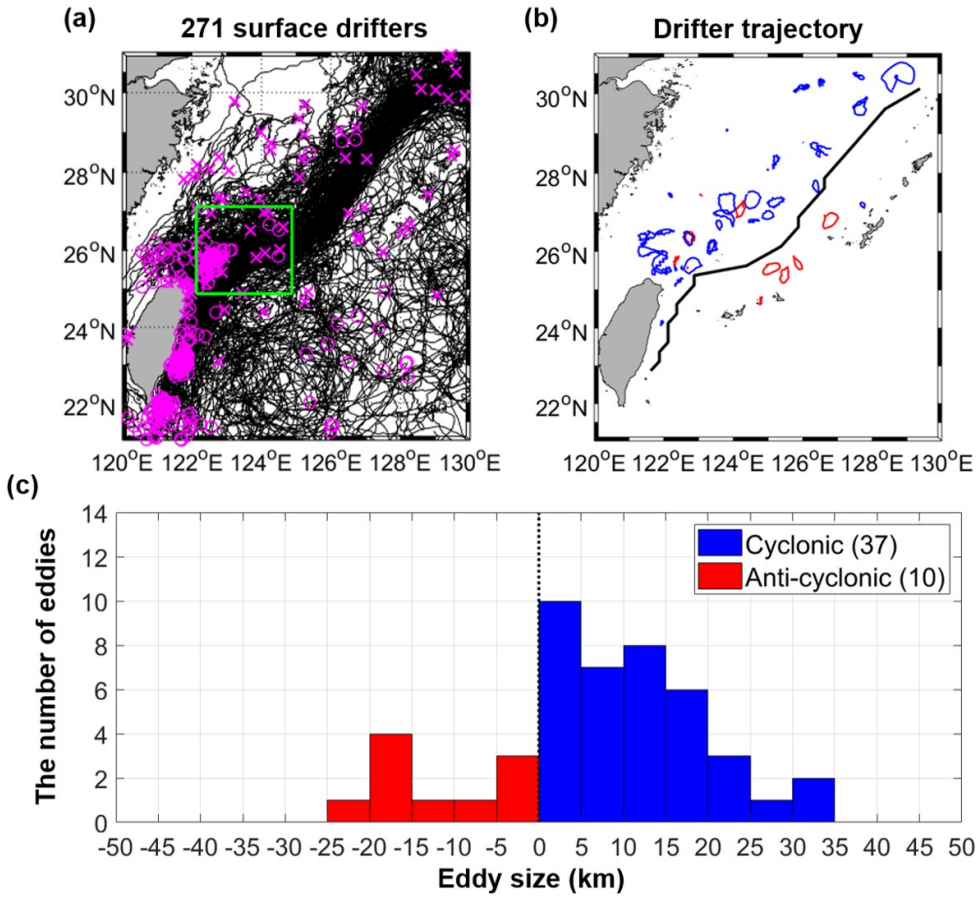

Figure 8. (a) Trajectories of the selected 271 surface drifters passed over the northeast of Taiwan (green box). The starting and ending positions are displayed with magenta circles and 'x' markers, respectively. **(b)** Trajectories of the eddies derived from the selected surface drifters by lagrangian eddy detection scheme of Dong et al. (2011). Blue and red lines are for cyclonic and anti-cyclonic eddies. The black line denotes the Kuroshio main axis. **(c)** Histogram of the number of eddies in terms of eddy size (radius) and spinning direction. Positive and negative values in the x-axis denote the cyclonic and anti-cyclonic eddies.

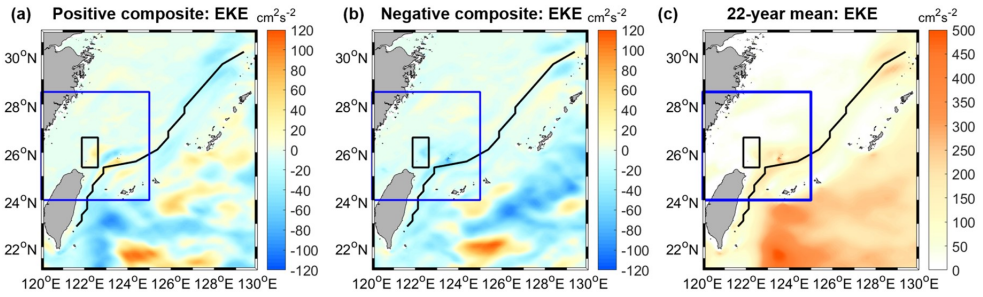

Figure 9. (a) Positive and **(b)** negative composite of eddy kinetic energy (EKE) anomalies, and **(c)** 22-year mean of the EKE from FORA-WNP30 reanalysis. The black boxes and black lines denote the KSI domain and the Kuroshio main axis. Blue boxes indicates the shelf region seen in Figure 13.

4. Discussion and Conclusions

This study investigated the interannual to decadal variability of the KSI and its associated changes over the ECS, and confirmed that the northeasterly wind stress, upward turbulent heat flux, SST shelf warming, and mesoscale EKE are strengthened during the KSI. The increase of northeasterly wind corresponds to the previous understanding that the wind-driven Ekman transport induces a westward shift of the Kuroshio (Guo et al., 2006). The onshore intrusion of the warm Kuroshio water is associated with the SST warming and increase of the upward heat flux over the ECS (Wang & Oey, 2014).

The main purpose of this study includes to advance the previous understanding by examining the KSI-associated changes in the subsurface temperature and sub-mesoscale eddy activity. The subsurface temperature changes differently in the deep western boundary current region and the shallow shelf region. While both the surface and subsurface experience warming over the deep Okinawa trough, the subsurface exhibits cooling in the continental shelf region during the KSI, which can be interpreted by topographic control; relatively cold deep water mass between A16 and A21 (Figure 7c) moves toward the ECS shelf and contribute to the decrease of the subsurface temperature in the shallow shelf region at depths of between 20 and 100 m. The composites of salinity anomalies display similar patterns in terms of depth (Figure 10) and vertical section of them (Figure 11). The

salinity decreases in the upper 40 m but increases in the continental shelf region during the KSI (Figure 11a). This features may be due to the topographic effect which is similar to the variability of the temperature according to the KSI. The saline deep water masses could move toward the shelf region (Figure 11c), then the salinity gets relatively higher than surrounding. However, the changes of temperature anomalies with the KSI occurrence are much more significant than those of salinity.

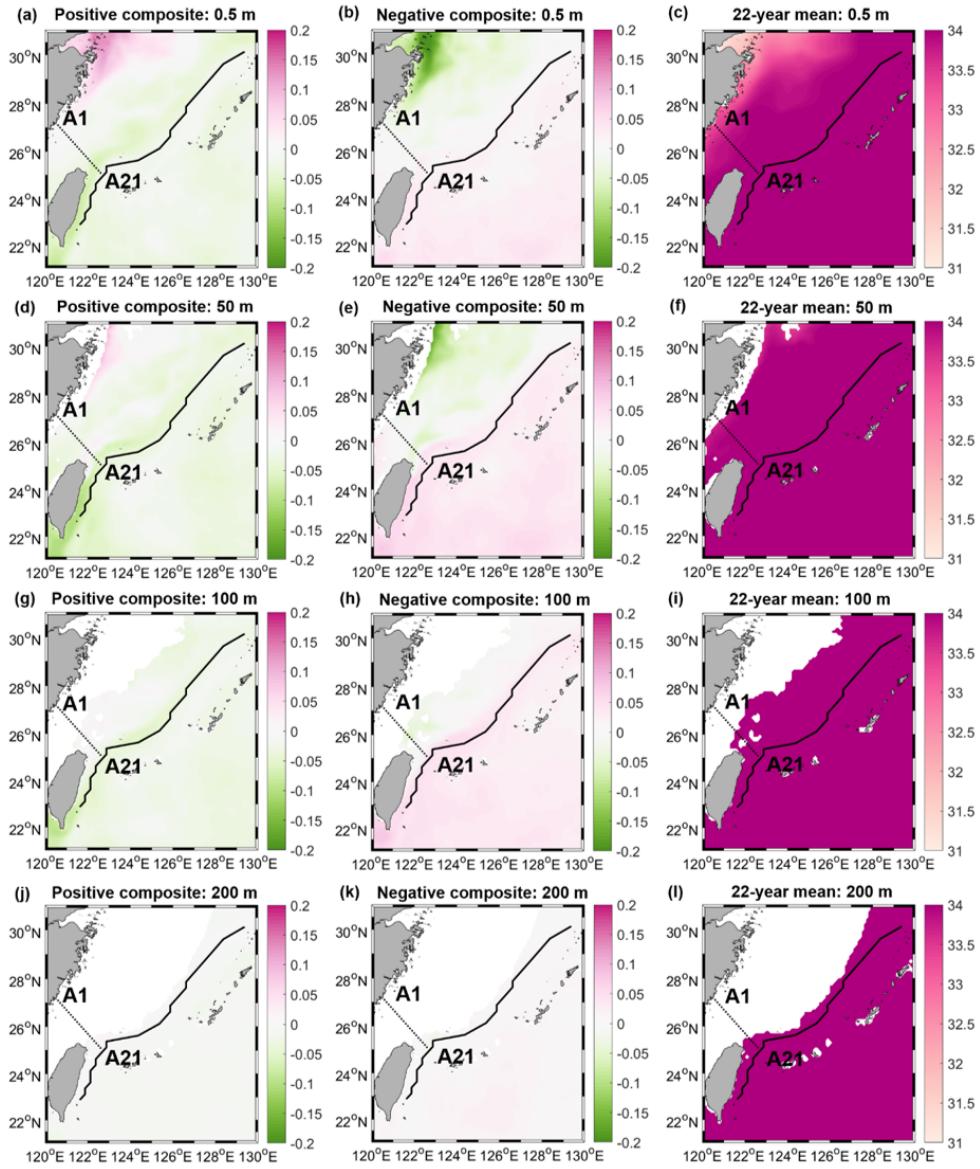

Figure 10. Positive and negative composites of salinity anomalies based on the KSIS index, and 22-year mean (1993–2014) of the salinity from FORA-WNP30 reanalysis. Line-A is aligned from A1 to A21. **(a-c)** 0.5 m. **(d-f)** 50 m. **(g-i)** 100 m. **(j-l)** 200 m. The black lines denote the Kuroshio main axis.

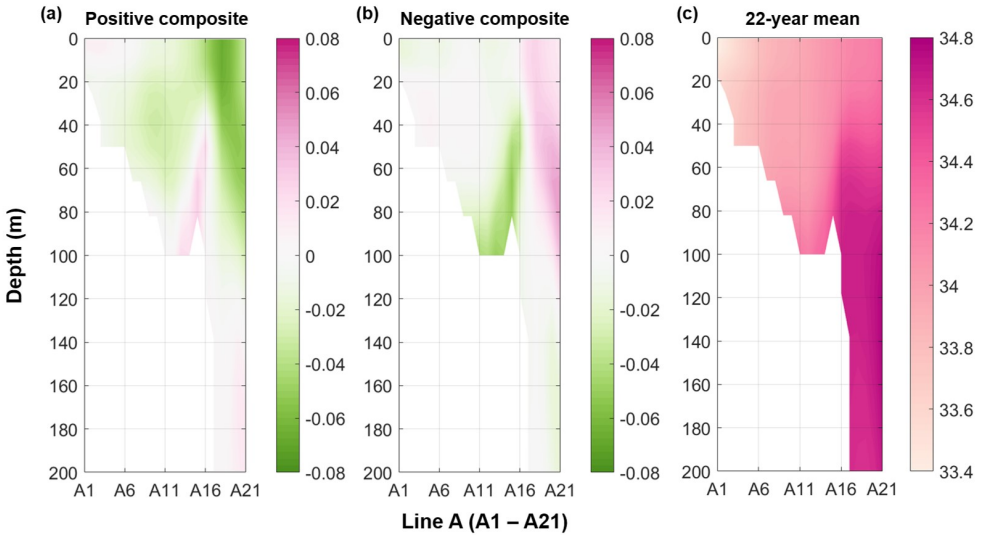

Figure 11. Vertical sections of **(a)** positive and **(b)** negative composites of salinity anomalies based on the KSIS index, and **(c)** 22-year mean of the salinity from FORA-WNP30 reanalysis. The line-A is shown in Figure 6.

The changes in the sub-mesoscale EKE was investigated after revisiting that there are more sub-mesoscale eddies than mesoscale eddies in the ECS by analyzing the surface drifter data. However, the GDP surface drifters are not steady in terms of time (Figure 12a) passing through the specific domain (Figure 8a). The surface drifters are concentrated in the time period of 2008–2009, thus, the detected eddies are restricted to the same period (Figure 8b).

Therefore, there is need to analyze the high-resolution ocean reanalysis in order to reveal the EKE including the sub-mesoscale variability. As shown in Section 3, variability of the sub-mesoscale EKE according to the KSI is more significantly than mesoscale EKE within an enlarged domain (Figure 13).The sub-mesoscale EKE relatively increases in the KSI domain and along the Kuroshio main axis but decreases in between them during the KSI (Figure 13d) compared to mesoscale EKE (Figure 13a). It could provide evidence of the Kuroshio shift toward the shelf region. However, the detailed physical mechanism of these changes is remained to be investigated further in future studies.

This study examined the KSI-associated changes based on the composite analysis by using the KSIS index. Although the composite maps showed overall opposite sings of anomalies between the KSI and non-KSI, they do not guarantee the cause and effect relationship with the KSI. With the help of the several previous studies, however, the relationship can be inferred between the KSI and other variables (e.g., winds, surface

temperature, heat flux, eddy activity). Furthermore, it would be an interesting study that discovers the environmental changes when the KSI continues over the years (e.g. 2000, 2001, 2005, and 2010) whereas the non-KSI is dominant (e.g., 1997, 1999, and 2016). Furthermore, the decadal variability which indicated between the period of 1995–1998 and 2006–2012 could be the future research.

The changes in the winds and mesoscale eddy activity east of Taiwan would induce the KSI, and the surface and subsurface temperature, surface heat flux, EKE inside the ECS change due to the KSI. The KSI thus would modulate interaction between the ocean and atmosphere, and hydrographic properties in the ECS. This study expands our previous understanding on the KSI variability and its associated oceanic changes from surface to subsurface, and also from mesoscale to sub-mesoscale variability, which would contribute to the study on the climate and ecosystem over the ECS.

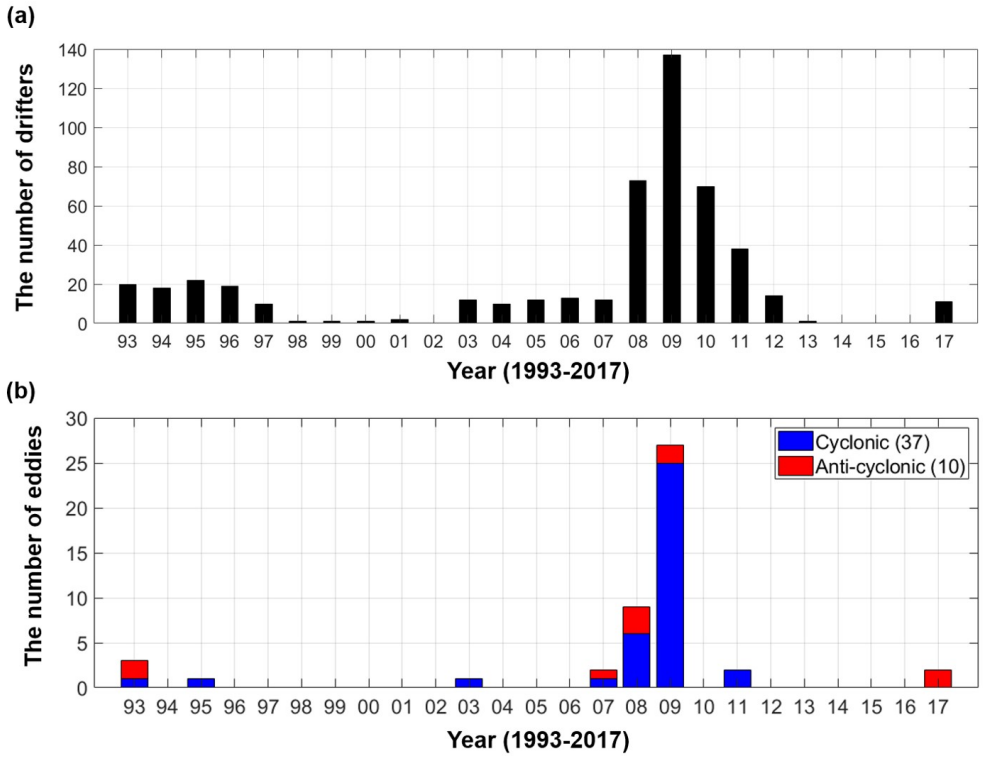

Figure 12. (a) The yearly number of surface drifters passed over the northeast of Taiwan. **(b)** The yearly number of eddies from the selected surface drifters.

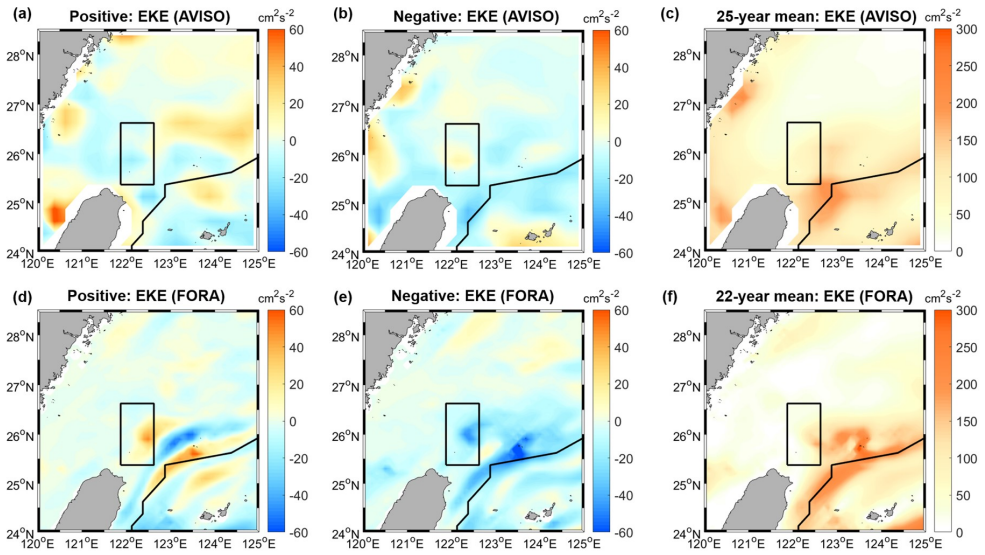

Figure 13. Comparison of mean EKE and EKE anomalies from satellite altimetry and FORA-WNP30 reanalysis over the shelf region of the ECS shown as blue boxes in Figures 5 and 9. **(a)** Positive and **(b)** negative composites of EKE anomalies, and **(c)** 25-year mean of the EKE from satellite altimetry. **(d)** Positive and **(e)** negative composites of EKE anomalies, and **(f)** 22-year mean of the EKE from FORA-WNP30 reanalysis. The black boxes and black lines denote the KSI domain and the Kuroshio main axis.

References

Andres, M., Park, J. H., Wimbush, M., Zhu, X. H., Nakamura, H., Kim, K., et al. (2009). Manifestation of the Pacific decadal oscillation in the Kuroshio. *Geophysical Research Letters,* 36, L16602, doi:10.1029/2009GL039216

Badin, G., Mahadevan, A., & Tandon, A. (2011). Lateral mixing in the pycnocline by baroclinic mixed layer eddies. *Journal of Physical Oceanography, 41*, 2080–2101.

Boccaletti, G., Ferrari, R., & Fox-Kemper, B. (2007). Mixed layer instabilities and restratification. *Journal of Physical Oceanography, 37,* 2228–2250, doi:10.1175/JPO3101.1

Chen, C. T. A., Ruo, R., Pai, S. C., Liu, C. L., & Wang, G. T. F. (1995). Exchange of water masses between the East China Sea and the Kuroshio off northeastern Taiwan. *Continental Shelf Research, 15*, 19–39.

Chen, C. C., Shiah, F. K., Chung, S. W., & Liu, K. K. (2006). Winter phytoplankton blooms in the shallow mixed layer of the South China Sea enhanced by upwelling. *Journal of Marine Systems, 59*(1–2), 97–110.

Chern, C. S., Wang, J., & Wang, D. P. (1990), The exchange of Kuroshio and East China Sea shelf water. *Journal of Geophysical Research, 95*(C9), 16,017–16, 023.

Chuang, W. S., & Liang, W. D. (1994). Seasonal variability of intrusion of the Kuroshio water across the continental shelf northeast of Taiwan. *Journal of Oceanography, 50*, 531–542.

Dong, C. M., Liu, Y., Lumpkin, R., Lankhorst, M., Chen, D., McWilliams, J. C., et al. (2011). A scheme to identify loops from trajectories of oceanic surface drifters: An application in the Kuroshio extension region. *Journal of Atmospheric and Oceanic Technology, 28*(9), 1167–1176, doi:10.1175/Jtech-D-10-05028.1

Dong, C., McWilliams, J. C., Liu, Y., & Chen, D. (2014). Global heat and salt transports by eddy movement. *Nat. Communications., 5*, 3294, doi:10.1038/ncomms4294

Gan, J.P., Wang, J. J., Liang, L. L., & Guo, X. G. (2015). A modeling study of the formation, maintenance, and relaxation of upwelling circulation on the northeastern South China Sea shelf. *Deep Sea Research, Part Ⅱ, 117*(SI), 41–52.

Guo, X., Hukuda, H., Miyazawa, Y., & Yamagata, T. (2003). A triply nested ocean model for simulating the Kuroshio-Roles of horizontal resolution on JEBAR. *Journal of Physical Oceanography, 33*, 146–169.

Guo, X. Y., Miyazawa, Y., & Yamagata, T. (2006). The Kuroshio onshore intrusion along the shelf break of the East China Sea: The origin of the Tsushima warm current. *Journal of Phyical Oceanography, 36*, 2205–2231, doi:10.1175/JPO2976.1

Guo, X., Zhu, X. H., Wu, Q. S., & Huang, D. (2012). The Kuroshio nutrient stream and its temporal variation in the East China Sea. *Journal of Geophysical Research, 117*, C01026, doi:10.1029/2011JC007292

Hu, J., & Wang, X. H. (2016). Progress on upwelling studies in the China seas. *Reviews of Geophysics, 54*, 653–673, doi:10.1002/2015RG000505

Hsin, Y. C., Qiu, B., Chiang, T. L., & Wu, C. R. (2013). Seasonal to interannual variations in the intensity and central position of the surface Kuroshio east of Taiwan. *Journal of Geophysical Research: Oceans, 118*, 4305-4316, doi:10.1002/jgrc.20323

Jan, S., Mensah, V., Andres, M., Chang, M. H., & Yang, Y. J. (2017). Eddy-Kuroshio interactions: Local and remote effects. *Journal of Geophysical Research: Oceans, 122*, 9744–9764. http://doi.org/10.1002/2017JC013476

Johns, W. E., Lee, T. N., Zhang, D., Zantopp, R., Liu, C. T., & Yang, Y. (2001). The Kuroshio east of Taiwan: Moored transport observations from the WOCE PCM-1 array. *Journal of Physical Oceanography, 31*, 1031-1053, doi:10.1175/1520-0485(2001)031<1031:TKEOTM>2.0.CO;2

Kamachi, M., Kuragano, T., Ichikawa, H., Nakamura, H., Nishina, A., Isobe, A., et al. (2004). Operational data assimilation system for the Kuroshio south of Japan: Reanalysis and validation. Journal of Oceanography, 60, 303–312.

Kamidaira, Y., Uchiyama, Y., & Mitarai, S. (2017). Eddy-induced transport of the Kuroshio warm water around the Ryukyu Islands in the East China Sea. *Continental Shelf Research, 143*, 206-218.

Lee, I. H., Ko, D. S., Wang, Y. H., Centurionim L., & Wang, D. P. (2013). The mesoscale eddies and Kuroshio transport in the western North Pacific east of Taiwan from 8-year (2003-2010) model reanalysis. *Ocean Dynamics, 63*, 1027–1040, doi:10.1007/s102360-0012-0643-z

Liu, Y., Dong, C., Guan, Y., Chen, D., McWilliams, J., & Nencioli, F. (2012). Eddy analysis in the subtropical zonal band of the North Pacific Ocean. *Deep-Sea Research, Part Ⅰ, 68*, 54–67.

Liu, Z. L., & Gan, J. P. (2012). Variability of the Kuroshio in the East China Sea derived from satellite altimetry data. *Deep Sea Research, Part Ⅰ, 59*, 25–36.

Liu, X., Dong, C., Chen, D., & Su, J. (2014). The pattern and variability of winter Kuroshio intrusion northeast of Taiwan. *Journal of Geophysical Research: Oceans, 119*, 5380–5394, doi:10.1002/2014JC009879

Liu, Y., Dong, C., Liu, X., & Dong, J. (2017). Antisymmetry of oceanic eddies across the Kuroshio over a shelfbreak. *Scientific Reports, 7*(1), 6761. https://doi.org/10.1038/s41598-017-07059-1

Lumpkin, R., & Centurioni, L. (2019). Global Drifter Program quality-controlled 6-hour interpolated data from ocean surface drifting buoys.

NOAA National Centers for Environmental Information. Dataset. http://doi.org/10.25921/7ntx-z961

Mensah, V., Jan, S., Chiou, M. D., Kuo, T. H., & Lien, R. C. (2014). Evolution of the Kuroshio tropical water from the Luzon Strait to the east of Taiwan. *Deep Sea Research, Part Ⅰ, 86*, 68–81, doi:10.1016/j.dsr.2014.01.005

Nitani, H. (1972). Beginning of the Kuroshio, Kuroshio: Its physical aspects edited by H. Stommel and K. Yoshida, pp. 129–163, University of Tokyo Press, Tokyo.

North, G. R. (1984). Empirical orthogonal functions and normal modes. *Journal of the Atmospheric Sciences, 41*, 879–887.

Oey, L. Y., Chang, M. C., Chang, Y. L., Lin, Y. C., & Xu, F. H. (2013). Decadal warming of coastal China Seas and coupling with winter monsoon and currents. *Geophysical Research Letters, 40*, 6288–6292, doi:10.1002/2013GL058202

Oey, L. Y., Chang, Y. L., Lin, Y. C., Chang, M. C., Varlamov, S., & Miyazawa, Y. (2014). Cross flows in the Taiwan Strait in winter. *Journal of Physical Oceanography, 44*, 801–817.

Qin, D., Wang, J., Liu, Y., & Dong, C. (2015). Eddy analysis in the eastern China Sea using altimetry data. *Frontiers of Earth Science, 9*(4), 709–721. http://doi.org/10.1007/s11707-015-0542-3

Sasaki, Y. N., & Yamada, Y. (2018). Atmospheric response to interannual variability of sea surface temperature front in the East China Sea in

early summer. *Climate Dynamics, 51*, 2509–2522. https://doi.org/10.1007/s00382-017-4025-y

Sassa, C., Konishi, Y., & Mori, K. (2006). Distribution of jack mackerel (Trachurus japonicas) larvae and juveniles in the East China Sea, with special reference to the larval transport by the Kuroshio Current. *Fisheries Oceanography, 15*(6), 508–518.

Soeyanto, E., Guo, X., Ono, J., & Miyazawa, Y. (2014). Interannual variations of Kuroshio transport in the East China Sea and its relation to the Pacific Decadal Oscillation and mesoscale eddies. *Journal of Geophysical Research: Oceans, 119*, 3595–3616, doi:10.1002/2013JC009529

Tang, T. Y., & Yang, Y. J. (1993). Low frequency current variability on the shelf break Northeast of Taiwan. *Journal of Oceanography, 49*, 193–210, doi:10.1007/BF02237288

Tang, T. Y., Hsueh, Y., Yang, Y. J., & Ma, J. C. (1999). Continental slope flow northeast of Taiwan. *Journal of Physical Oceanography, 29*(6), 1353–1362, doi:10.1175/1520-0485(1999)029<1353:CSFNOT>2.0.CO;2

Usui, N., Wakamatsu, T., Tanaka, Y., Hirose, N., Toyoda, T., Nishikawa, S., et al. (2017). Four-dimensional variational ocean reanalysis: A 30-year high-resolution dataset in the western North Pacific (FORA-WNP30). *Journal of Oceanography, 73*(2), 205–233. http://doi.org/10.1007/s10872-016-0398-5

Vélez-Belchí, P., Centurioni, L. R., Lee, D. K., Jan, S., & Niiler, P. P. (2013). Eddy induced Kuroshio intrusions onto the continental shelf of the East China Sea. Journal of Marine Research, 71, 83–108.

Wang, J., & Oey, L.Y. (2014). Inter-annual and decadal fluctuations of the Kuroshio in East China Sea and connection with surface fluxes of momentum and heat. *Geophysical Research Letters, 41*, 8538-8546, doi:10.1002/2014GL062118

Wang, Y. L., Wu, C. R., & Chao, S. Y. (2016). Warming and weakening trends of the Kuroshio during 1993–2013. *Geophysical Research Letters, 43*, 9200–9207, doi:10.1002/2016GL069432

Wu, C. R. (2013). Interannual modulation of the Pacific Decadal Oscillation (PDO) on the low-latitude western North Pacific. Progress in Oceanography, 49–58, doi:10.1016/j.pocean.2012.12.001

Wu, C. R., Hsin, Y. C., Chiang, T. L., Lin, Y. F., & Tsui, I. (2014). Seasonal and interannual changes of the Kuroshio intrusion onto the East China Sea Shelf. *Journal of Geophysical Research: Oceans, 119*, 5039–5051, doi:10.1002/2013JC009748

Wu, C. R., Wang, Y. L., Lin, Y. F., & Chao, S. Y. (2017). Intrusion of the Kuroshio into the South and East China Seas. *Scientific Reports, 7*(1), 7895. http://doi.org/10.1038/s41598-017-08206-4

Xie, S. P., Xie, Q., Wang, D., & Liu, W. T. (2003). Summer upwelling in the South China Sea and its role in regional climate variations. *Journal of Geophysical Research: Oceans, 108*(C8), 3261,

doi:10.1029/2003JC001867

Yang, Y., Liu, C. T., Hu, J. H., & Koga, M. (1999). Taiwan current (Kuroshio) and impinging eddies. *Journal of Oceanography, 55*, 609–617.

Yang, D. Z., Huang, R. X., Yin, B. S., Feng, X. R., Chen, H. Y., Qi, J. F., et al. (2018a). Topographic beta spiral and onshore intrusion of the Kuroshio Current. *Geophysical Research Letters, 45*, 287–296. http://doi.org/10.1002/2017GL076614

Yang, D. Z., Yin, B. S., Chai, F., Feng, X., Xue, H., Gao, G., et al. (2018b). The onshore intrusion of Kuroshio subsurface water from February to July and a mechanism for the intrusion variation. *Progress in Oceanography, 167*, 97–115. http://doi.org/10.1016/j.pocean.2018.08.004

Yin, Y., Lin, X., He, R., & Hou, Y. (2017). Impact of mesoscale eddies on Kuroshio intrusion variability northeast of Taiwan. *Journal of Geophysical Research: Oceans, 122*, 3021–3040, doi:10.1002/2016JC012263

Yin, Y., Lin, X., & Hou, Y. (2019). Seasonality of the Kuroshio intensity east of Taiwan modulated by mesoscale eddies. *Journal of Marine Systems, 193*, 84–93.

Zhang, D., Lee, T. N., Johns, W. E., Liu, C. T., & Zantopp, R. (2001). The Kuroshio east of Taiwan: Modes of variability and relationship to interior ocean mesoscale eddies. *Journal of Physical Oceanography,*

31, 1054–1074.

Zhu, J., Chen, C., Ding, P., Li, C., & Lin, H. (2004). Does the Taiwan warm current exist in winter? *Geophysical Research Letters, 31*, L12302. https://doi.org/10.1029/2004GL019997

국문 초록

동중국해 쿠로시오 대륙붕 유입의 장주기 변동성

강지원

지구환경과학부

서울대학교 대학원

동중국해에서 쿠로시오 해류가 오키나와 골 서쪽 대륙붕 방향으로 치우치는 현상을 쿠로시오 대륙붕 유입(Kuroshio shelf intrusion; KSI)이라고 한다. 이는 대륙붕 해역과 서안경계류 해역 사이의 수괴 교환을 일으키고, 동중국해 주변 생태계와 기후에 큰 영향을 미친다. KSI는 대만 동쪽 쿠로시오 해류가 약해질 때 나타나며, 여름철에 비해 겨울철에 더욱 빈번하게 발생한다고 알려져 있다. 본 연구는 KSI의 경년 및 십년 주기 변동 특성을 밝히기 위해 인공위성 고도계, 고해상도 재분석장 결과, 표층 뜰개와 같은 다양한 자료를 이용하여 동중국해에서 일어나는 KSI와 관련된 해양 변화를 분석하였다. Composite 분석을 통해 KSI 현상이 동중국해 해역의 북동풍 강화, 해양에서 대기로의 열 방출 증가,

표층 수온 증가와 관련되어 있음을 확인하였다. 쿠로시오 주축이 대륙붕 쪽으로 이동함에 따라 수심이 깊은 오키나와 골 부근에서는 아표층 수온 역시 증가하지만, 수심이 얕은 대륙붕 해역 아표층에서는 지형 효과로 인해 수온이 오히려 감소하는 것으로 나타났다. 또한 KSI 가 일어날 때 중규모 소용돌이의 운동에너지 변화보다 아중규모 소용돌이의 운동에너지 변화가 쿠로시오 주축 부근과 대륙붕 해역에서 더 크게 나타났다. 본 연구는 동중국해의 기후와 생태계에 영향을 주는 KSI 현상에 관한 기존 연구를 표층에서 아표층으로, 중규모 변동에서 아중규모 변동으로 확장하여 경년 및 십년 주기의 KSI 변동 및 이와 관련된 변화를 이해하는데 기여하였다.

주요어: 쿠로시오 대륙붕 유입, 동중국해, 아표층 수온, 아중규모 소용돌이, 소용돌이 운동 에너지

학번: 2018-25621